Thermal Stability of Magnetron Sputter Deposited NiZr Alloys for Hydrogen Gas Separation

V. Gorokhovsky[a], K. Coulter[a], T. Barton[b], S.Swapp[c]

[a]Southwest Research Institute, San Antonio Texas USA
[b]Western Research Institute, Laramie, Wyoming, USA
[c]University of Wyoming, Laramie, Wyoming, USA

Keywords: hydrogen, membrane, amorphous metal, sputtering, thermal stability

Abstract

Thin film amorphous alloy membranes are a promising new technology for hydrogen separation. The ultimate goal of the project is to produce amorphous metallic membranes on porous stainless steel supports. NiZr amorphous alloys have shown promise but their low crystallization temperature limits their use in power plants. In this study, NiZr alloy films were deposited by co-sputtering from magnetrons with nickel and zirconium targets. The NiZr films were characterized by EDS and RBS for elemental composition and XRD and SEM for phase composition, structure and morphology. It was found that an increase in Zr content in films from 3 to 30 at. % induces a dramatic reduction in crystal size making this alloy almost amorphous at 15-30 at.% of Zr. The films with higher Zr content were further examined for their thermal stability. The fabrication, characterization, and potential application of NiZr alloy thin films as hydrogen separation membranes is discussed.

Introduction

Amorphous alloy membranes based on a combination of early transition metals and late transition metals are an alternative to current platinum group metal (PGM) membranes, offering hydrogen permeance and selectivity that is comparable to palladium alloys, plus the potential advantages of high resistance to crystalline hydride formation and lower cost [1]. H_2 separation membranes based on amorphous metals are generally more attractive than their crystalline equivalents because they typically exhibit improved mechanical and structural properties without concern for defect-free film growth. This is primarily a result of the fact that these structured materials are readily stabilized in alloy form. Amorphous metals are commonly reported to exhibit increased strength, ductility, corrosion resistance, and, more importantly, H_2 solubility [2] than their crystalline analogues. Furthermore, they usually contain a more open lattice which decreases the embrittlement dangers associated with H_2 purification [3]. Amorphous metallic H_2 membranes are capable of withstanding repeated cycling, high temperatures, and high pressures, all of which are common operating conditions for industrial scale H_2 separations. This class of membrane material offers the additional advantage of outstanding compositional flexibility and homogeneity and high catalytic surface activities for enhanced H_2-surface interactions [4]. These properties can be composition dependent, as is the case for the amorphous nickel-based alloys: $(Zr_{36}Ni_{64})_{1-x}(Ti_{39}Ni_{61})_x$ and $(Zr_{36}Ni_{64})_{1-x}(Hf_{36}Ni_{64})_x$, where $0 < x < 1$ and which required catalytic surface coatings to lower the surface activation energies. In contrast, $Zr_{36}Ni_{64}$ does not

require a catalytic surface coating [5]. The local structure of amorphous metals, which can be described via a radial distribution function (RDF) may affect hydrogen diffusivity and permeability as was found by Density Functional Theory (DFT) modeling [17].

Bulk metal glasses (BMG) can be produced by many different techniques such as rapid solidification of overcooled metal liquids, metal attrition by ball milling, or fast melting of the surface of metal by laser or e-beam source [11,17,18]. Melt-spun ribbons of a NiNbZr amorphous alloy have been produced by the single-roller melt-spinning technique [18]. Amorphous metal thin films can be produced by multi-elemental deposition using various vacuum coating techniques including ion plating, magnetron sputtering and laser ablation [8-10]. The ion bombardment of growing film during deposition is crucial for amorphization of the metal alloy film [12]. The energy of bombardment may range from 5-10 eV to 100s of eV, but it must exceed the characteristic energy of the atoms in a lattice. Suitable ion bombardment assistance during deposition can be achieved by utilizing the energy of sputtering atoms ranging from 1 to 10 eV or, alternatively, a separate ion source can be used for bombardment of the growing film in ion beam assisted deposition (IBAD) processes [12]. The amorphous metal films of different compositions were successfully deposited by magnetron co-sputtering technique with and without additional ion beam assistance [8-10]. It was found that by exposing the substrate in turn to different magnetron sputtering flows, it is possible to form nanolaminated films or films with modulated concentrations of different metal components of the multielemental metal film. The energy of sputtering atoms or additional ion bombardment by an independent ion source was found to be a critical issue in amorphization of the nanolaminated multielemental films and formation of amorphous metal coatings. The solid state amorphization reactions can also play a role in amorphization of multielemental metal alloys as was discovered in references [13-16]. In this case the multilayer film employing either a sequence of bi-layers of two different metals is subjected to annealing below their re-crystallization temperature. When the Gibbs energy of a metastable amorphous state is lower than that of polycrystalline state the amorphous phase can be formed via interfacial solid-state reactions without any rapid quenching [15]. The essential factors which permit such a reaction are the fast diffusion behavior of one of metal in the other, and the existence of a negative heat of mixing in the amorphous alloy. Both of these factors are satisfied in NiZr based alloys as was reported in [16]. The aim of this work was to study composition-related structure, physical properties and thermal stability of amorphous metal thin film coatings prepared by vacuum coating deposition process in comparison with BLG materials.

Experimental

The coating system setup used in this work is shown in **Figure 1**. Two DC magnetrons using 4" diameter targets were installed at the bottom of the vacuum processing chamber for a co-sputtering deposition process of the amorphous alloy with argon as the processing gas. The magnetrons were equipped with Ni and Zr targets for deposition of a Ni_xZr_{1-x} alloy coating of various compositions. The substrate-holding turntable was installed above the magnetrons at the distance of 15 cm from the magnetron targets and rotated at 12 RPM. Prior to the coating deposition process, substrates were pre-heated to 300^{o}C by a radiant heater. At the end of the heating stage, the RF bias (50W, 120 volts autopolarization potential) was applied to the substrate turntable. The RF bias of the substrates was used only during the ion cleaning stage. Substrate pre-heating was applied only during the substrate conditioning stage prior to the coating deposition stage. The argon pressure during pre-heating and RF-ion cleaning stages was 10 mtorr. When the coating deposition stage started, both substrate bias and substrate heater were

turned off. Coatings were applied to stainless steel disc samples 1" diameter, 1/8" thick and/or 1"×1" lime glass coupons. The substrate setup includes six coupons which were placed evenly around the axes of the substrate table. Two of these coupons were masked for measurement of coating thickness using the step method with a VEECO Dektak 150 precision profilometer. The argon pressure during coating deposition stage was 3 mTorr. The deposition duration was either 1 or 2 hrs resulting in a coating thickness ranging from ~3 to 8 μm. The morphology of the deposited coatings was studied by SEM and optical micro-imaging. Coating composition was studied by EDS and RBS techniques. Ion beam analysis of the coated samples was performed using a 2 MV van de Graaff accelerator at Montana State University. It utilized He+ and H+ beams up to 2 MeV. Composition profiles were determined by comparing SIMNRA computer simulations of the spectra with the original data [6,7]. Crystallinity of the samples was examined by glancing angle x-ray diffractometer. A Hysitron NanoIndentor was utilized for attaining the measurements of the hardness and elastic modulus of the deposited metal films. Giving the thickness of the films, the Hysitron's load settings were adjusted in order to give an indentation of approximately 300 nanometers. The initial calibrations for the machine were performed at the desired depth and were carried out on a fused mica sample. The bulk electrical resistivity of the coatings was measured by the voltage drop between two contact electrodes made of copper foil attached to opposite ends of the deposited film when the constant current of 100 mA was applied. Sample annealing was conducted on stainless trays in a stainless steel tube furnace in an argon/2% hydrogen atmosphere.

Results and Discussion

NiZr coating composition can be estimated from the respective deposition rates of Ni and Zr coatings by the following expression:

$$m(Zr)/m(Ni)= \dot{c}(Zr)/\dot{c}(Ni), \quad (1)$$

where m is mass fraction of the metal, $\dot{c}$ is deposition rate of the metal. This expression and technical approach was proven during the preliminary trials. The linear extrapolations of the deposition rates of the magnetrons equipped with Zr and Ni targets vs. respective magnetron powers are shown in **Figure 2**. In addition, the figure shows the estimated combined Ni+Zr deposition rate, calculated with assumption that $\dot{c}(Ni_xZr_{1-x})= \dot{c}(Ni)+\dot{c}(Zr)$.

Ni_xZr_{1-x} coatings of various compositions were deposited by co-sputtering from two magnetrons by changing the deposition rates of Zr and Ni by varying the respective magnetron powers similar to the process used in [8,9]. The compositions of the coatings deposited during different process runs using various combinations of applied magnetron powers are shown in **Table 1**. Fractional concentrations of Zr and Ni in the selected coatings measured by EDS and RBS techniques have shown nearly identical results, so the less expensive EDS technique was used for the rest of the coatings studied in this work. Deposition rates and Ni concentrations in Ni_xZr_{1-x} coating vs. Ni magnetron power at 100W Zr magnetron power are shown in **Figure 3**. The figure shows a nearly linear relationship between coating compositions and deposition rates vs. applied magnetron power. Comparing the deposition rate of Ni_xZr_{1-x} deposited at both magnetron powers near 250W (Sample # 11, **Table 1**) with calculated deposition rate presented in **Figure 2**, shows additive behavior of co-sputtered coatings with no considerable influence of molar volume change associated with formation of Ni_xZr_{1-x} solid solution. This can be explained by the fact that in co-sputtering process performed in this work, with magnetrons positioned at a

substantial distance from each other, the coating is forming rather as a nanolaminated multilayer architecture than a solid solution of metal components deposited by different magnetrons. In this case, the deposition rate of co-sputtered Ni_xZr_{1-x} films can be estimated as a sum of the deposition rates of Ni and Zr films deposited by respective magnetron powers.

As illustrated in **Figure 4,** NiZr coatings deposited by co-sputtering have demonstrated a dense morphology with no pin-holes or porosity. Hardness and elastic modulus of the sputtered deposited Ni_xZr_{1-x} coatings have a strong correlation with their composition as shown in **Figure 5**. The minimal hardness and elastic modulus appears near a Zr content of 16 at %. The toughness of these coatings also reaches a minimum value near 15 at % of Zr followed by increase with increase of the Zr content, reaching the maximum value in the coatings having near optimal Zr content of about 30 at % associated with a fully amorphous NiZr alloy [5,16,17,18].

XRD analysis of the crystallinity of NiZr coatings and ribbons has demonstrated a strong correlation between their structure and thermal stability vs. their composition. The first three samples presented in **Table 1** (samples #1-3) have relatively small Zr content, less than 10 at %. The intense, broad peak near 44^o 2-θ appears for all these three samples. The full width at half maximum intensity (FWHM) for an XRD spectra taken from these samples indicates the broadening of the 44^o 2-θ peak with an increase of Zr in the coatings. In addition, a second, low-intensity peak at approximately 2.5^o 2-θ appears in two samples (samples 2 and 3m **Table 1**) with the smallest Zr content indicating the possibility of formation of other polycrystalline phases in these samples. The FWHM continues broadening with an increase of the Zr content in samples #4-11 from **Table 1** reaching the maximum value in samples #10 and #11 with Zr content near 30 at % as can be seen in **Figure 6**. The XRD patterns of these samples closely resemble the XRD pattern obtained from $Ni_{0.64}Zr_{0.36}$ ribbon prepared by rapid quench melt-spun technique. All as-deposited samples #1, 4-11 having Zr content >9 at % have demonstrated the broad XRD peak with a shape typical for amorphous metal alloys.

Annealing of the samples and ribbons for 1 hour at 200^oC results in no re-crystallization as illustrated in **Figure 7**. Broadening of the 44^o 2-θ peak in sample coating #1 can indicate further amorphization of this film by a solid amorphization reaction via fast interdiffusion between the Ni rich and Zr rich sub-layers, which may happen in this nanolaminated coating during annealing below the re-crystallization temperature via the amorphization mechanism reported in Ref. [16]. Coatings with higher concentrations of Zr have survived annealing for 1 hour at 250^oC without re-crystallization as can be seen from **Figure 8**. The re-crystallization started during 1 hr of annealing at 300^oC in coatings with lower Zr content (sample #1), while coatings with Zr content > 12 at % do not re-crystallize, showing XRD patterns after annealing similar to the melt-spun ribbon with optimal Zr content associated with amorphous NiZr alloy as shown in **Figure 9** ($Ni_{0.64}Zr_{0.36}$ ribbon sample # 12 in **Table 1**). On the other hand, the ribbon sample #13 having $Ni_{0.3}Zr_{0.7}$ composition was fully transformed into the polycrystalline state after 1 hr of annealing at 300^oC. The optimal composition of the NiZr amorphous alloys with Zr concentration near 30 at % is in agreement with other work presented in Refs. [5,17,18].

Coatings and ribbons which demonstrated the best thermal stability when exposed to short-term annealing were further tested by annealing for 24 hrs at 300^oC. The results of this test are shown in **Figure 10**. It can be seen that three sample coatings (samples 9, 10 and 11 from **Table 1**) and a melt-spun ribbon sample #12 with near optimal Ni:Zr ratios show the mixture of polycrystalline phase with amorphous matrix after annealing for 24 hours at 300^oC. Among these samples the coating #11 with the $Ni_{0.71}Zr_{0.29}$ composition and the ribbon #12 with the $Ni_{0.64}Zr_{0.36}$ composition demonstrated almost identical XRD patterns after 24 hours of annealing at 300°C.

This result demonstrates that both a thin film coating deposited by co-sputtering and BMG ribbons prepared by the melt-spun technique have a similar thermal stability that is determined by their elemental composition and not by their fabrication technique.

The electrical resistivity in thin films is very sensitive to their structure. Electrical resistivities of polycrystalline Ni and Zr metals are 6.99×10^{-6} Ohm.cm and 42.4×10^{-6} Ohm.cm, respectively. Using this data, the electrical resistivity ρ of the polycrystalline Ni_xZr_{1-x} films can be estimated based on a simplistic mechanical mixture model which can be expressed by the following equation:

$$\rho\ (Ni_xZr_{1-x}) = x\rho_{Ni} + (1-x)\rho_{Zr}, \quad (2)$$

Both electrical conductivities of as-deposited Ni_xZr_{1-x} films and the values of their electrical resistivities calculated from Eqn. 2 are presented in **Figure 11**. It can be seen that the electrical resistivity of as-deposited Ni_xZr_{1-x} films increased with Zr content and achieved up to two times greater than that of pure Zr at a Zr content of 29 at. % when the coating was fully amorphous. In addition, the electrical resistivity of the as-deposited coatings is approximately 4 to 5 times greater than that calculated as a mixture of respective polycrystalline metals (Eqn. 2). The electrical resistivity of amorphous metal alloys is generally greater than that in a polycrystalline state due to the increase in electron scattering on grain boundaries of nano-sized grains within the amorphous metals [8-10].

Table 1: Fractional Elemental Concentrations and Deposition Rates of Ni_xZr_{1-x} Films

Sample #	Substrate	Zr magnetron power, W	Ni magnetron power, W	Deposition rate, μm/hr	x (EDS) Ni_xZr_{1-x}	x (RBS) N_xZr_{1-x}
1	glass	100	350	3.3	0.9	0.91
2	glass	100	400	3.4	0.92	0.92
3	glass	100	450	3.85	0.93	0.93
4	glass	100	200	2.1	0.84	0.85
5	glass	100	275	2.7	0.88	0.89
6	SS	100	275	2.7	0.87	
7	SS	150	275	2.8	0.81	
8	SS	150	275	2.8	0.82	
9	glass	150	275	3.0	0.82	
10	glass	200	275	3.1	0.76	
11	glass	250	275	3.4	0.71	
12	Melt-spun ribbon	N/A	N/A	N/A	0.64	
13	Melt-spun ribbon	N/A	N/A	N/A	0.3	

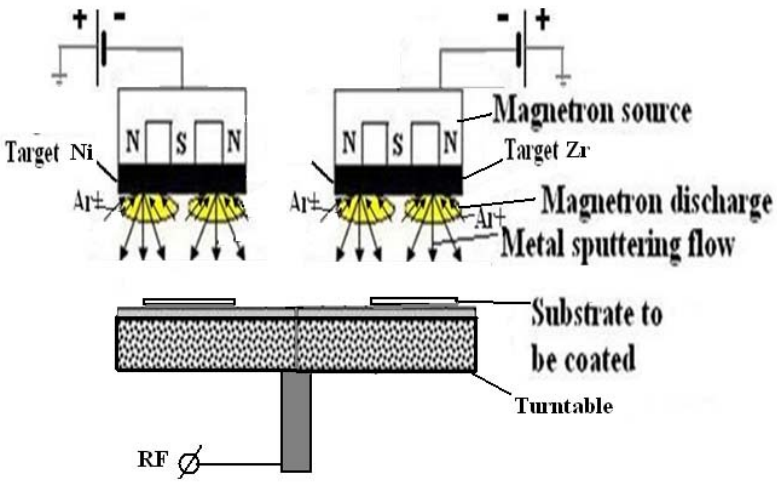

Figure 1. Magnetron co-sputtering scheme

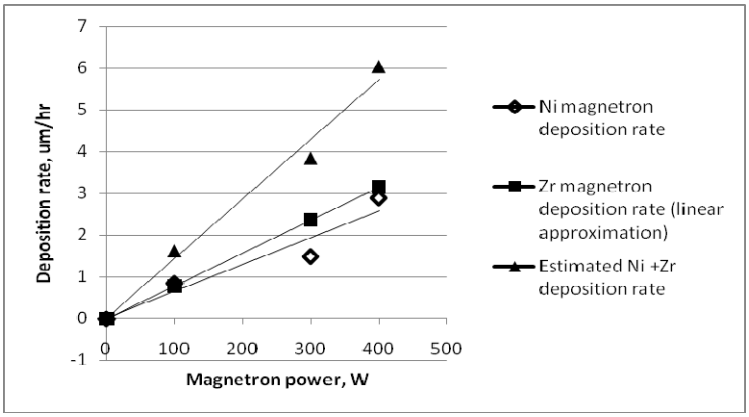

Figure 2. Deposition rates of Ni and Zr vs. magnetron power.

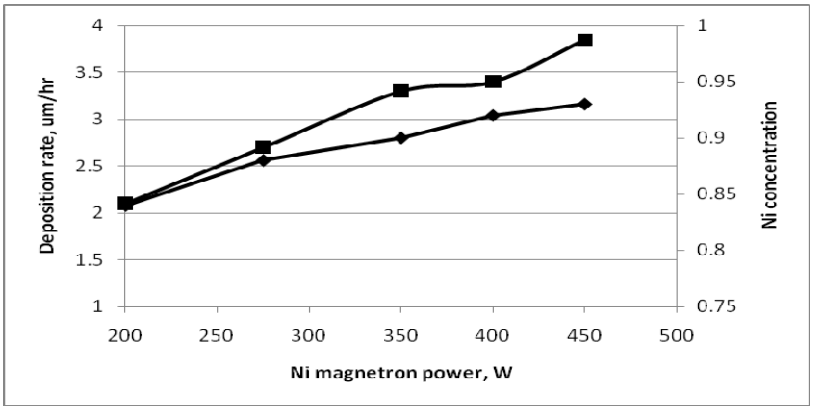

Figure 3. Deposition rate and Ni concentration in of Ni_xZr_{1-x} coating vs. Ni magnetron power at Zr magnetron power fixed at 100W.

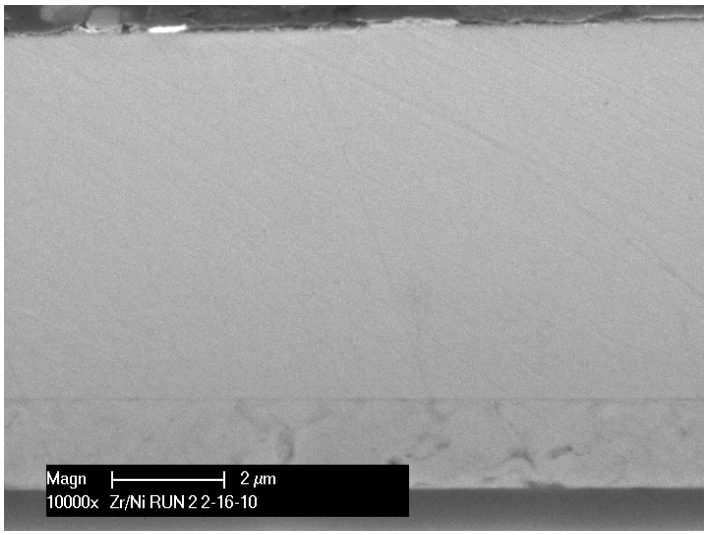

Figure 4. SEM micrograph of the cross-section of $Ni_{0.93}Zr_{0.07}$ coating.

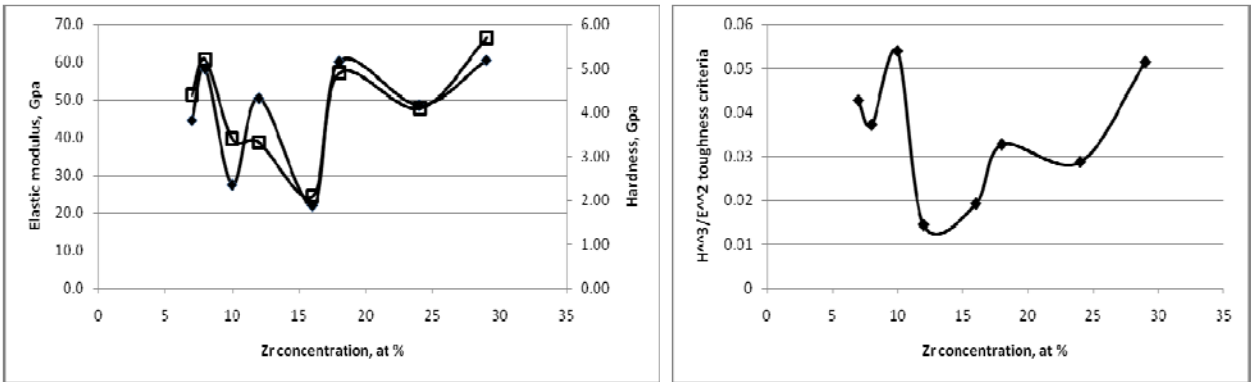

Figure 5. Mechanical properties of as deposited Ni_xZr_{1-x} coatings vs. coating composition: hardness and elastic modulus (left); H3/E2 toughness parameter(right)

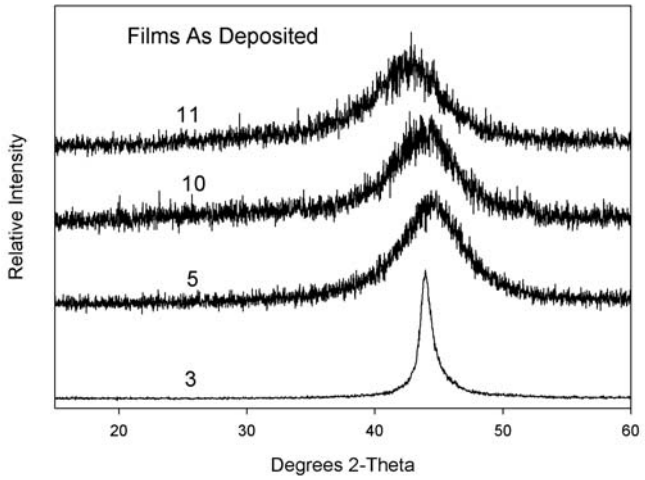

Figure 6. XRD patterns of as deposited Ni_xZr_{1-x} coatings.

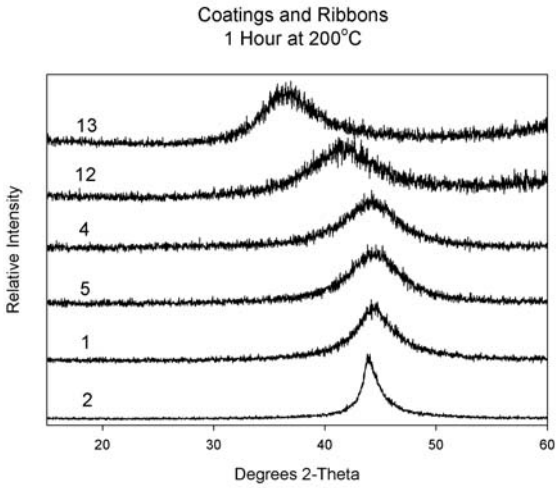

Figure 7. XRD patterns of Ni_xZr_{1-x} coatings subjected to 1 hour annealing at 200˚C.

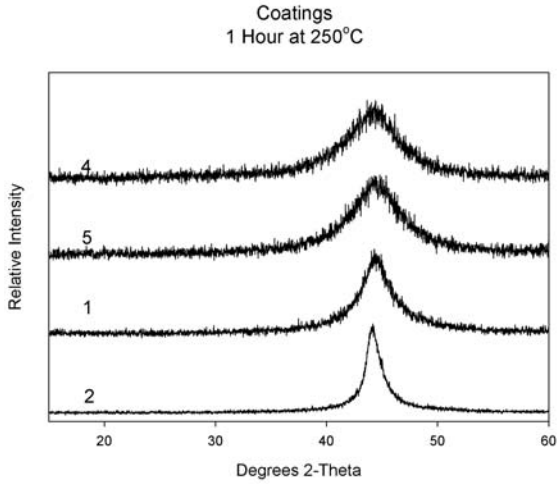

Figure 8. XRD patterns of Ni_xZr_{1-x} coatings subjected to 1 hour annealing at 250˚C.

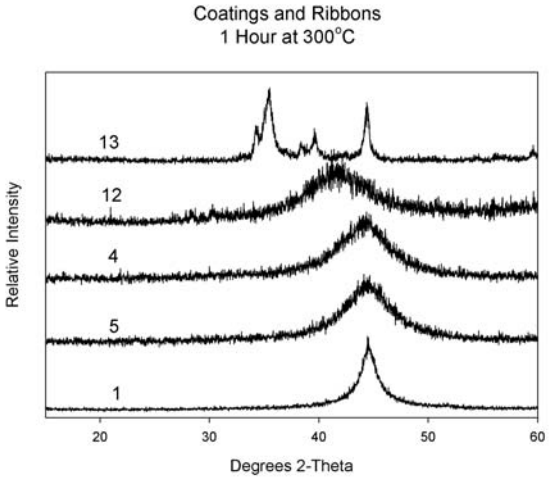

Figure 9. XRD patterns of Ni_xZr_{1-x} coatings and BMG ribbons subjected to 1 hour annealing at 300˚C.

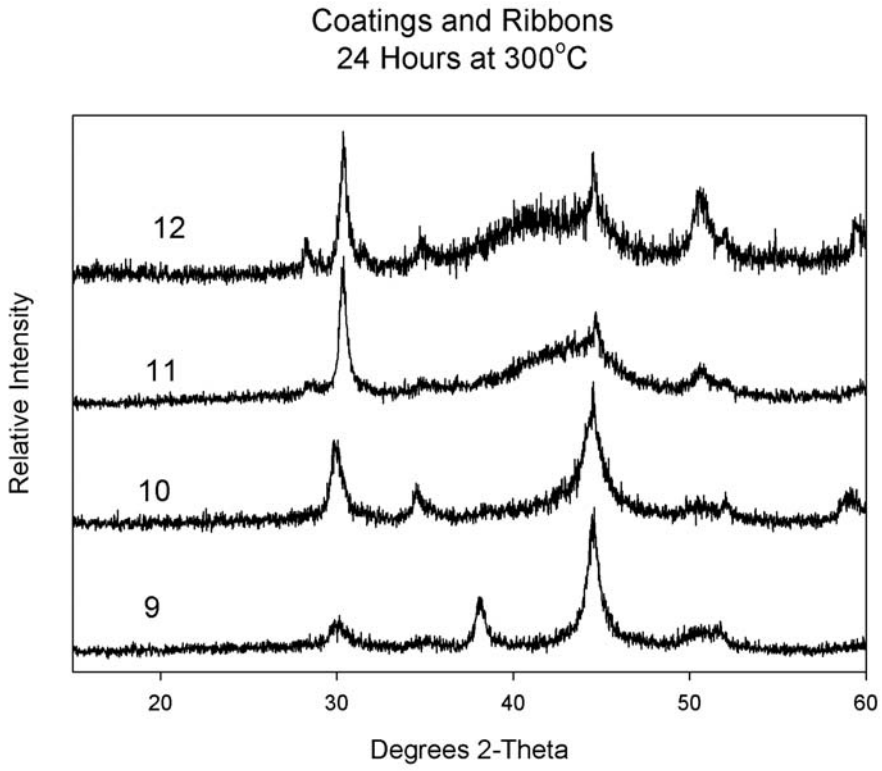

Figure 10. XRD patterns of Ni_xZr_{1-x} coatings and BMG ribbon subjected to 24 hours annealing at 300˚C.

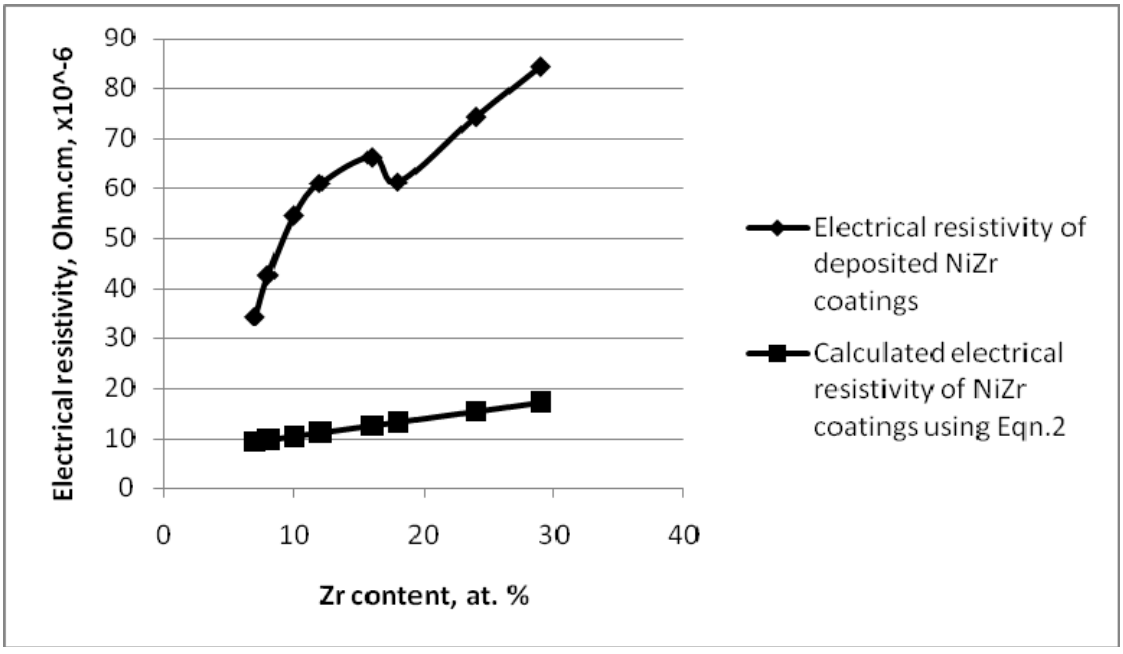

Figure 11. Electrical conductivity of as deposited Ni_xZr_{1-x} coatings.

Conclusions

Ni_xZr_{1-x} coatings with x ranging from 0.71 to 0.93 were deposited by magnetron co-sputtering process. It was found that as-deposited films are more amorphous with an increase of Zr content starting from x = 0.9 and reaching a XRD-amorphous state at x > 0.88. Mechanical properties of these coatings are strongly correlated with their composition. Amorphous films with higher Zr content have retained their XRD measured amorphous state after 1 hr annealing in an argon/2% hydrogen atmosphere at 300°C. Further amorphization of some of the coatings, with lower Zr content, occur during thermal annealing below their re-crystallization temperature which may indicate the influence of a solid reaction amorphization mechanism on the coating structure evolution. The partial re-crystallization in films with the highest Zr content occurs after 24 hours of annealing. The $Ni_{0.71}Zr_{0.29}$ coating has demonstrated the best thermal chemical stability developing a mixture of a polycrystalline phase embedded within an amorphous matrix during annealing. The XRD spectrum of this film is nearly identical to the XRD spectrum of a melt-spun BMG ribbon subjected to the same annealing treatment, indicating that thin film coatings deposited by co-sputtering and BMG ribbons prepared by the melt-spinning technique have about the same thermal stability which is determined by their elemental composition and not by the method of fabrication. Future work will be conducted to better understand the mechanisms of formation of amorphous metal coatings and their thermal stability, which is critical for their applications in hydrogen separation membranes.

Acknowledgments

We acknowledge Jim Riggs who skillfully prepared the coatings, Byron Chapa for SEM characterization and Forrest Campbell for electrical measurements of the coatings, and Richard Smith for RBS analysis. The authors thank David Sholl and Darius Milcius for valuable discussions on amorphous metal membranes. Special thanks to Dhanesh Chandra for providing samples of melt-spun NiZr BBMG ribbons for comparative study. This work was supported by DOE under contract No. DE-FE-0001057 and supervised by DOE project officer Steven Markovich.

References

[1] M.D. Dolan, N.C. Dave, A.Y. Ilyushechkin, L.D. Morpeth and K.G. McLennan, Composition and operation of hydrogen-selective amorphous alloy membranes, *J. Membr. Sci.,* 285, 2006, p 30-55.

[2] N.W. Ockwig and T.M. Nenoff, Membranes for Hydrogen Separation, *Chem. Rev.,* 107, 2007, p 4078-4110.

[3] S. Hara, K. Sakaki, N. Itoh, H.M. Kimura, K. Asami and A. Inoue, An amorphous alloy membrane without noble metals for gaseous hydrogen separation, *J. Membr. Sci.*, 164, 2000, p 289-294.

[4] Y. Zhang, T. Ozaki, A. Komaki, and C. Nishimura, Hydrogen permeation of Pd–Ag alloy coated V–15Ni composite membrane: effects of overlayer composition, *J. Membr. Sci.,* 224, 2003, p 81-91.

[5] S. Hara, N. Hatakeyama, N. Itoh, H.M. Kimura, and A. Inoue, Hydrogen permeation through

amorphous-Zr36−xHfxNi64-alloy membranes, *J. Membr. Sci.*, 211, 2003, p 149-156.

[6] M. Mayer, SIMNRA User's Guide, Technical Report IPP 9/113, Max-Planck-Institut fur Plasmaphysik, Garching, Germany, (1997).

[7] J.R. Tesmer, M. Nastasi, Handbook of Modern Ion Beam Materials Analysis, Materials Research Society, Pittsburgh, PA, 1995.

[8] Aleksandras ILJINAS, Sigitas JONELIŪNAS, Darius MILČIUS, Julius DUDONIS, "Deposition of Amorphous Fe-Zr Alloys by Magnetron Co-sputtering," MATERIALS SCIENCE (MEDŽIAGOTYRA). Vol. 13, No. 2. 2007p.117-119.

[9] J. Dudonis, R. BruCas, A. Miniotas, **"**Synthesis of amorphous Zr-Cu alloys by magnetron co-sputtering**,"** *Thin Solid Films*, 275, 1996, p 164-167.

[10] D. Horwat, M. Dehmas, E. Aubry, J. Zollinger, S. Migot, J.F. Pierson, "Properties of nanocrystalline and nanocomposite WxZr1_x thin films deposited by co-sputtering," *Intermetallics*, 17, 2009, p 421-426.

[11] A. Inoue, X.M. Wang, W. Zhang, "DEVELOPMENTS AND APPLICATIONS OF BULK METALLIC GLASSES," *Rev. Adv. Mater. Sci.*, 18, 2008, p 1-9.

[12] D. Milcius, C. Templier, J. P. Riviere, L.L. Pranevicius, L. Pranevicius, "High-flux, low-energy implantation effects on the composition of altered layers," *Surface and Coatings Tech.,* 156, 2002, p 214-218.

[13] R.B. Schwarz, W.L. Johnson, "Formation of an Amorphous Alloy by Solid-State Reaction of the Pure Polycrystalline Metals," *Phys. Rev. Lett.*, 51, 1983, p 415.

[14] R.B. Schwarz, "Formation of Amorphous Alloys by Solid State Reactions," *Matl. Sci. Eng.*, 1988, Vol. 97, p 71-78.

[15] K. Samwer, "Amorphisation in solid metallic systems," *Physics Reports*, Vol. 161, Is.1, 1988, p 1-41.

[16] W.J. Meng, C.W. Vieh, E. Ma, B. Fultz, W.L. Johnson, "Solid state interdiffusion reactions of Ni/Zr Diffusion Couples," *Matl. Sci. Eng.*, 1988, v.97, p.87-91.

[17] S. Hao, D.S. Sholl, "Comparison of first-principles calculations and experiments for hydrogen permeation through amorphous ZrNi and ZrNiNb films," J. Membrane Science, 2010.

[18] S.I. Yamaura, Y. Shimpo, H. Okouchi, M. Nishida, O. Kajita and A. Inoue, "The effect of additional elements on hydrogen permeation properties of melt-spun Ni-Nb-Zr amorphous alloys", *Mater. Trans.*, 45, 2004, p 330-333.